THE JOURNAL OF BIOLOGICAL CHEMISTRY VOL. 282, NO. 37, pp. 26675–26686, September 14, 2007

Activation of Targeted Necrosis by a p53 Peptide

*A NOVEL DEATH PATHWAY THAT CIRCUMVENTS APOPTOTIC RESISTANCE**

Received for publication, March 2, 2007, and in revised form, June 19, 2007 Published, JBC Papers in Press, July 18, 2007, DOI 10.1074/jbc.M701864200

Richard D. Dinnen[‡], Lisa Drew[‡], Daniel P. Petrylak[‡], Yuehua Mao[‡], Nicholas Cassai[§], Joseph Szmulewicz[§], Paul Brandt-Rauf[¶], and Robert L. Fine[‡1]

From the [‡]Experimental Therapeutics Program, Division of Medical Oncology, Columbia University, College of Physicians and Surgeons, New York, New York 10032, the [¶]Department of Environmental Health Sciences, Mailman School of Public Health, Columbia University, College of Physicians and Surgeons, New York, New York 10032, and the [§]Department of Pathology and Laboratory Medicine, Harbor Veterans Affairs Medical Center, SUNY Downstate Medical Center, Brooklyn, New York 11203

Cancer cells escape apoptosis by intrinsic or acquired mechanisms of drug resistance. An alternative strategy to circumvent resistance to apoptosis could be through redirection into other death pathways, such as necrosis. However, necrosis is a nonspecific, nontargeted process resulting in cell lysis and inflammation of both cancer and normal cells and is therefore not a viable alternative. Here, we report that a C-terminal peptide of p53, called p53p-Ant, induced targeted necrosis only in multiple mutant p53 human prostate cancer lines and not normal cells, because the mechanism of cytotoxicity by p53p-Ant is dependent on the presence of high levels of mutant p53. Topotecan- and paclitaxel-resistant prostate cancer lines were as sensitive to p53p-Ant-induced targeted necrosis as parental lines. A massive loss of ATP pools and intracellular generation of reactive oxygen species was involved in the mechanism of targeted necrosis, which was inhibited by O_2^- scavengers. We hypothesize that targeted necrosis by p53p-Ant is dependent on mutant p53, is mediated by O_2^- loss and ATP, and can circumvent chemotherapy resistance to apoptosis. Targeted necrosis, as an alternative pathway for selective killing of cancer cells, may overcome the problems of nonspecificity in utilizing the necrotic pathway.

The currently accepted paradigm is that most anticancer agents, at clinically relevant concentrations, act by inducing cell death in cancer cells via pathways of apoptosis. Therefore, anticancer agents are developed to maximize apoptosis. However, cancer cells eventually become resistant to therapeutic agents that induce caspase-dependent apoptosis. There are multiple specific mechanisms that may contribute to resistance to apoptosis not only in prostate cancer cells but virtually all cancer cells, which include changes in Bcl-2 (1), p53 (2, 3), p21 (4), and a myriad of other changes (5, 6). Therefore, disabling just one of the prior mechanisms of resistance may not render sensitivity to cancer cells, because of the multiple, redundant anti-apoptotic mechanisms that exist concomitantly within cancer cells (7).

In the search for more effective therapies, possible avenues to examine are alternate death pathways, which bypass resistance mechanisms of apoptosis. Necrosis is one alternate pathway, with fewer mechanisms of resistance compared with apoptosis. But because it is a nonspecific process resulting in cell lysis and inflammation of cancer and normal cells, necrosis has not generally been considered a viable alternative to apoptosis. However, it maybe possible to exploit necrosis, specifically against cancer cells, by induction of what we termed "targeted necrosis" (8). Targeted necrosis has potential clinical utility, because its cell death mechanism retains the cancer cell specificity of apoptosis and bypasses apoptotic resistance by redirection into necrosis.

The molecular mechanisms of necrosis have not been well defined, but it can occur as a result of an incomplete execution of apoptosis (9). Necrosis and apoptosis share some common pathway elements (10), and often the same stimulus can direct a cell into either mode of death (11). Apoptosis requires energy through ATP, whereas necrosis is an ATP-independent mechanism of cell death. Therefore, one primary factor that determines whether a cell follows an apoptotic or necrotic pathway is the intracellular concentration of ATP (9, 12). The absence of sufficient energy reserves can switch cells from an apoptotic to a necrotic form of death. Poly(ADP-ribose) polymerase (PARP)[2] has been proposed as one of the switch points that determines whether a cell undergoes apoptosis (when PARP is cleaved and inactivated, not depleting ATP pools), or necrosis (when PARP is not cleaved and remains active) (13). Lack of PARP cleavage through inhibition of caspases (14) or activation of PARP can ultimately cause necrosis by depletion of ADP-ribose leading to decreased ADP pools to form ATP (13).

* This work was supported in part by NCI, National Institutes of Health Grant RO1-85828 and by a Herbert Pardes Scholar Award, the Manelski Family Foundation, the R. C. Hayes Foundation Award, and a Herbert Irving Scholar Award (to R. L. F.), a Prostate Cancer Foundation grant (to D. P. P.), and National Institutes of Health Grant R01-OH07590 (to P. B.-R.). The costs of publication of this article were defrayed in part by the payment of page charges. This article must therefore be hereby marked "*advertisement*" in accordance with 18 U.S.C. Section 1734 solely to indicate this fact.

This work is dedicated to the memory and courage of Michael Rothman, who died of prostate cancer.

[1] To whom correspondence should be addressed: Experimental Therapeutics, Division of Medical Oncology, Columbia University, College of Physicians and Surgeons, 650 West 168th St., BB 20-05, New York, NY 10032. Tel.: 212-305-1168; Fax: 212-305-7348; E-mail: rlf20@columbia.edu.

[2] The abbreviations used are: PARP, poly(ADP-ribose) polymerase; Anx V, Annexin V; Ant, 17-amino acid peptide from *D. antennapedia* homeobox domain; BOC-Asp-FMK, tertiary-butyloxycarbonyl-aspartate-fluoromethylketone; LDH, lactate dehydrogenase; DCFDA, 5(and 6) carboxy-2′,7′-dichloro-dihydrofluorescein diacetate; MnTMPyP, Manganese (III) tetrakis (1-methyl-4-pyridyl) porphyrin; MTT, 3-[4,5-dimethylthiazol-2-yl]-2,5-diphenyl tetrazolium bromide; O_2^-, superoxide free radical; PAC, Paclitaxel; PI, propidium iodide; ROS, reactive oxygen species; aa, amino acid(s); wt, wild type; TUNEL, deoxynucleotidyltransferase-mediated dUTP nick end labeling; PBS, phosphate-buffered saline; shRNA, small hairpin RNA.

TABLE 1
Peptide amino acid sequences

Peptide	Sequence
Ant	N-KKWKMRRNQFWVKVQRG-C (17 aa)
p53p	N-[361]GSRAHSSHLKSKKGQSTSRHKK[382]-C (22 aa)
p53p-Ant[a]	N-**GSRAHSSHLKSKKGQSTSRHKK**WKMRRNQFWVKVQRG-C (37 aa)
p53p-Ant-RhoB	N-**GSRAHSSHLKSKKGQSTSRHKK**WKMRRNQFWVKVQRGK-(RhoB)-C (38 aa)
p53p-AntCONT	N-[372]**KKGQSTSR**[379]KKWKMRRNQFWVKVQRG-C (25 aa)

[a] p53p-Ant has 37 aa instead of 39 aa because the last two aa of p53p and the first two aa of Ant are KK; thus the KK of Ant was deleted. The p53p-ANTCONT has the full 17-aa sequence of Ant.

Our laboratory has been investigating the action of a p53 C-terminal 22-aa peptide (p53p, aa 361–382), linked to a truncated 17-aa peptide from the *Drosophila antennapedia* homeobox domain (Ant) to facilitate cellular uptake (p53p-Ant). This peptide induced classical apoptosis in several colon and breast carcinoma and Burkitt's lymphoma lines with mutant p53 (15–17). We found the mechanism of apoptosis by p53p-Ant was through a nontranscriptional/nontranslational, Fas/caspase-3 and -8-dependent pathway with cleavage of PARP (17). p53p-Ant induced classical apoptosis in multiple human carcinoma cell lines expressing mutant p53 but not in null p53 tumor lines. Nonmalignant human colon and breast cell lines expressing low levels of wt p53 were unaffected by peptide, but premalignant, mutant p53 colon and breast cell lines underwent Fas-mediated apoptosis from peptide (17, 18). Thus, the ability of the peptide for induction of apoptosis was directly correlated to levels of endogenous p53. We found that the binding target site of the peptide was at the tetramerization domain of p53 (18). Further studies in our lab with peptide and purified wt and mutant p53 in surface plasmon resonance (Biacore) studies revealed potent dissociation constants (K_d = $\sim 10^{-12}$ M) for mutant p53, whereas the K_d for wt p53 was weaker ($\sim 10^{-10}$ M). This may explain why p53p-Ant was not toxic to null p53 cells, normal cells, and CD34+ pluripotent marrow stem cells, which have either no p53 or low levels of wt p53 (18).

In this paper we report that p53p-Ant, when exposed to hormone-refractory, mutant p53 prostate cancer cell lines, induced primarily necrosis with some aborted features of apoptosis (9). Our hypothesis is that the mechanism of targeted necrosis is specific for mutant p53 prostate tumor cells and can overcome resistance to apoptosis by redirection to a necrotic pathway whose mechanism depends on the generation and toxic effects of superoxide (O_2^-).

EXPERIMENTAL PROCEDURES

Materials—C-terminal p53 peptide (aa 361–382) (p53p), Ant, p53p-Ant, and p53p truncated control (aa 372–379) (p53-AntCONT) peptides were chemically synthesized by Research Genetics (Huntsville, AL) and high pressure liquid chromatography-purified to more than 95% pure as previously described (17). p53p-Ant-Rhodamine B (RhoB) was synthesized by SynPep (Dublin, CA). Table 1 shows the peptides respective aa sequences. Peptide stocks (4 mM) were prepared in distilled water and stored in aliquots at −80 °C. Chemical antioxidants included Tiron (Aldrich) and MnTMPyP (Calbiochem, San Diego, CA). The antibodies included the N-terminal-derived human anti-p53 monoclonal antibody (clone DO-1, epitope: 11–25 aa), anti-PARP (F-2) (Santa Cruz, CA), and C-terminally derived anti-p53 monoclonal antibody (clone PAb421, epitope: aa residues 371–380) (Calbiochem, San Diego, CA).

Cell Culture—We worked with nine different human prostate cell lines and types. The human androgen-independent prostate cancer cell lines PC-3 (null p53), DU-145 (mutant p53, Leu-223 and Phe-274), 22R*v*1 (mutant p53, Arg-331), VCaP (mutant p53, Trp-248), and LNCaP (wt p53) were obtained from ATCC (Manassas, VA). The stably transfected, temperature-sensitive mutant p53 PC-3 cell line was made in our lab as described below under "Plasmids and Stable Transfection." P69 immortalized normal prostate cells were generously supplied by Dr. Paul Fisher (Columbia University). P69 cells were allowed to adhere to cell culture dishes for up to 4 h in RPMI medium containing 5% fetal bovine serum, 2 mM glutamine, 50 ng/ml gentamycine (Invitrogen), 0.1 μM dexamethasone, and ITS premix (BD Biosciences). The medium was then changed to RPMI containing 2 mM glutamine, 50 μg/ml gentamycine, 0.1 μM dexamethasone, ITS premix, and 1 μg/liter EGF (BD Biosciences). DURC-1 cells were generously supplied by Dr. Panayotis Pantazis (University of Miami). The DURC-1 cell line were parental DU-145 cells made resistant to camptothecin (CPT-11) and topotecan (19). Paclitaxel (PAC)-resistant DU-145 (DU-Tax-R) cells were generated in our lab by increasing the concentration of PAC in the medium over several months. Monolayer cultures were maintained in RPMI 1640 medium (Invitrogen) supplemented with 10% heat-inactivated fetal bovine serum (Atlanta Biologicals, Norcross, GA), 100 units/ml penicillin G, 100 μg/ml streptomycin, and 2 mM glutamine (Invitrogen) at 37 °C in a humidified atmosphere of 5% CO_2. For experiments, the cells were trypsinized and allowed to adhere overnight prior to treatment in medium containing 5% fetal bovine serum. For caspase inhibition experiments, the pan-caspase inhibitor BOC-Asp-FMK (Enzyme Systems Products, Livermore, CA) or Me_2SO vehicle control (final concentration, ≤0.1%) was added 30 min prior to treatment with peptide.

Plasmids and Stable Transfection—Plasmids of pCMV and pCMV/mutant temperature-sensitive p53-143 were a kind gift of Dr. Albert Deisseroth (Sidney Kimmel Cancer Center, La Jolla, CA). The plasmids were transfected into PC-3 cells by using Lipofectamine (Invitrogen). The selection of clones was carried out for 2 weeks with 800 μg/ml G418 (Invitrogen). The insertion of the temperature-sensitive p53-143 cDNA was determined by Western blot. The cells were maintained at 37 °C (mutant p53 conformation).

Western Blotting Analysis—Following treatment, the cells were collected by centrifugation at 2,000 × *g* for 5 min. The cell lysates were prepared in lysis buffer (20 mM Tris-Cl, pH 7.6, 1 mM EDTA, pH 8.0, 150 mM NaCl, 1% Triton X-100, 10 μg/ml

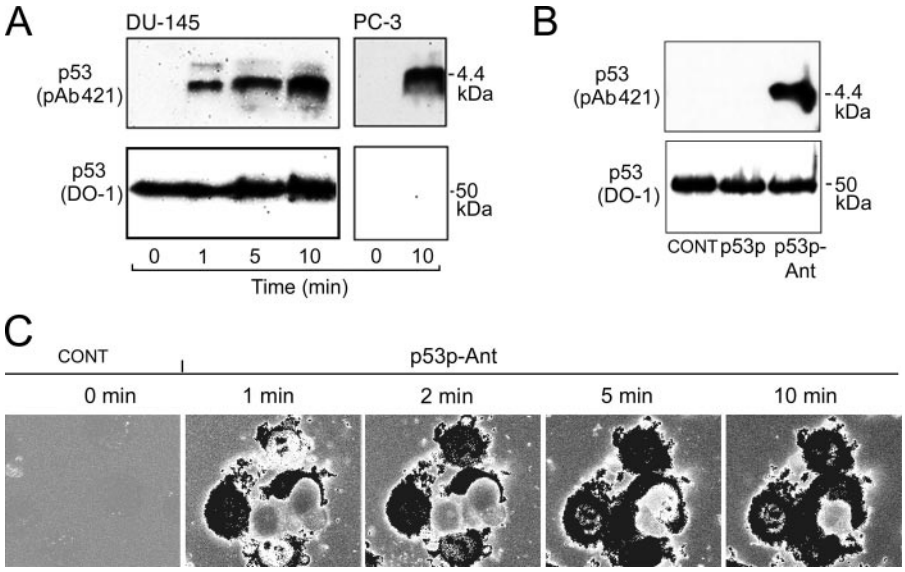

FIGURE 1. **p53p-Ant uptake.** *A*, DU-145 or PC-3 cells exposed to 30 μM p53p-Ant for up to 10 min. Anti-p53 pAb421 antibody (epitope 371–380 aa) detects peptide. The blots were stripped and reprobed with anti-p53 DO-1 antibody (epitope 11–25 aa) to confirm endogenous p53 status. *B*, DU-145 cells were untreated (*CONT*) or incubated with 30 μM p53p or p53p-Ant for 10 min. The cell lysates were analyzed as above. *C*, DU-145 cells incubated with 30 μM p53p-Ant-RhoB and fluorescence monitored by confocal microscopy. The same group of cells was followed for up to 10 min. Untreated cells showed no staining. Low intensity fluorescence is represented by *gray* (background color), medium intensity is *white*, and high intensity is *black*.

aprotinin, 1 mM benzamidine, 50 μg/ml leupeptin, 10 μg/ml pepstatin A, and 1 mM phenylmethylsulfonyl fluoride) for 15 min on ice and centrifuged at 10,000 $\times$ *g* for 10 min. The lysates (50 μg) were boiled in SDS sample buffer and loaded on SDS-PAGE. After transferring, immunoreactive products were detected by ECL system (Amersham Biosciences). Actin or α-tubulin was used as a control.

Peptide Uptake—p53p-Ant uptake into cells was determined by Western blotting and by monitoring uptake of rhodamine B conjugated to the C terminus of the peptide (p53p-Ant-RhoB). The cells were placed on a confocal microscope with 30 μM p53pAnt-RhoB, and uptake was monitored over time. Thirty μM p53pAnt was the IC_{50} concentration for induction of apoptosis in human mutant p53 breast and colon cancer lines (17, 18).

shRNA—shRNA constructs pAd/U6/p53-shRNA and pAd/U6/shuffled-p53-shRNA were inserted into an E1/E3-deleted adenovirus vector (20) and propagated in 293A cells according to the manufacturer's instructions (Invitrogen). The virus particle titer after filtration-based concentration (Adeno-X virus purification kit; Clontech) was 1×10^9 pu/ml as determined by plaque titration assay in 293A cells. DU-145 cells in log phase were infected for 48 h with pAd/U6/p53-shRNA or pAd/U6/shuffled-p53-shRNA at a multiplicity of infection of 4, 10, or 20. After infection, the cells were split, allowed to adhere overnight, and exposed to p53p-Ant for 6 h, and annexin V (Anx V) analysis was performed (see below).

Flow Cytometric Analysis for PI, TUNEL, ROS, Anx V, and Cell Surface Fas—The cells were incubated in the indicated concentration of peptides for up to 6 h unless otherwise stated. Following treatment, floating and adherent cells were harvested, washed, and resuspended in PBS. For PI analysis, the cells were fixed in ice-cold 70% ethanol, washed in PBS, and incubated with PI staining buffer (10 μg/ml PI and 250 μg/ml RNAse A) (Sigma) for 30 min at 25 °C. For TUNEL analysis, the cells were fixed in 4% paraformaldehyde for 30 min on ice, washed, and fixed in ice-cold 70% ethanol, washed, and incubated with fluorescein-dUTP and terminal deoxynucleotidyl transferase using the Mebstain apoptosis kit direct (MBL International, Watertown, MA). For ROS measurements, 10 μM DCFDA (2′,7′-dichlorodihydrofluorescein diacetate or 10 μM dihydroethidium (DHE) (Molecular Probes, Eugene OR) (for $O_2^{\cdot-}$) was added in the final 30 min of incubation. The cells were then scraped off the plate, washed, and resuspended in PBS. Fluorescein isothiocyanate-conjugated mouse anti-human monoclonal Fas/CD95 antibody (PharMingen, San Diego, CA) were used to determine cell surface Fas. For combined Anx V/PI analysis, floating and trypsinized cells were pooled and exposed to Alexa Fluor 488 (Molecular Probes) in binding buffer. PI stain was added (final concentration, 3.3 μg/ml) for 1 min and analyzed on a FACSCalibur flow cytometer (Becton Dickinson) and quantified using CELLQuest software. The fluorescent intensity of 10,000 cells were analyzed for PI, and 5000 cells were analyzed for TUNEL, ROS, Anx V, and Fas.

Assays for Nucleosomes, Caspase-3 and 8 Activity, ATP, LDH, and MTT—For all assays, the cells were seeded overnight and then incubated with peptides as indicated. All of the assays utilized pooled floating and trypsinized adherent cells and were performed according to the manufacturer's instructions. Cytoplasmic mono- and oligonucleosomes were determined using the enzyme-linked immunosorbent assay for nucleosomes (Roche Applied Science). Caspase-3 or caspase-8 protease activity were determined using colorimetric assay kits (MBL International, Watertown, MA). For intracellular ATP determination, the cells were collected and resuspended in ddH_2O and boiled for 5 min. Intracellular ATP levels were determined using a TD 20/20 luminometer (Turner Designs, Sunnyvale CA) at 560 nm using an ATP determination kit (Molecular Probes). The LDH assay was performed using a CytoTox 96 nonradioactive cytotoxicity assay for LDH release into the extracellular space (Promega). The maximal LDH release control was obtained by two rounds of freeze-thawing of cells, which fractured the plasma membrane of virtually all cells under the microscope. The MTT assay was performed using a cell proliferation kit (Roche Applied Sciences).

Cytotoxicity Analysis by Fluorescence Viability Assay—For determination of necrotic cells after peptide treatment, the cells were initially seeded onto poly-D-lysine-coated coverslips (Becton Dickinson). At the indicated times after peptide treatment,

the coverslips were removed and exposed to Calcein AM and Ethidium homodimer-1 using a live/dead viability/cytotoxicty kit (Molecular Probes) according to the manufacturers' instructions with pictures taken under a fluorescence microscope, and at least 300 cells were counted per time point by a blinded observer.

Confocal and Electron Microscopy—For confocal microscopy, the cells were initially seeded for 24 h in glass-bottomed plates (MatTek Corporation). Following treatment with 30 μM p53p-Ant-RhoB for the indicated times, the cells were viewed (Zeiss LSM 410 confocal laser scanning microscope). For electron microscopy, adherent and floating cells were collected, washed in PBS, and fixed with 2.5% gluteraldehyde-PBS. The fixed cells were rinsed in a 0.1 M phosphate buffer (pH 7.3), postfixed in 2% osmium tetroxide-PBS (pH 7.3), dehydrated in a graded series of ethanol and propylene oxide, and embedded in Epon 812. Sections were cut at 700 Å, stained with uranyl acetate and lead citrate, and examined with a Jeol JEM 1010 transmission electron microscope.

RESULTS

Uptake of p53p-Ant—Ant transduces peptides across plasma and nuclear membranes in a non-cell type-specific manner. Therefore, we investigated by Western blotting whether p53p-Ant could transduce DU-145 cells using the anti-p53 antibody PAb421. Immunoblotting of p53p-Ant alone without cells produced a band of 4.4 kDa (data not shown). A 4.4-kDa band was detected in DU-145 lysates. Similar results were found for PC-3 cells (Fig. 1*A*). The 4.4-kDa band was not observed in DU-145 cells incubated with p53p alone without Ant (Fig. 1*B*). The blots were stripped and reprobed with the anti-p53 N-terminal DO-1 antibody, which recognizes p53 but not the p53p-Ant epitope. This confirmed p53 expression in DU-145 cells, which has mutant p53, and confirmed that PC-3 cells were null for p53 (Fig. 1, *A* and *B*).

To determine subcellular localization of p53p-Ant, live cells were incubated with p53p-Ant-RhoB, and fluorescence was monitored in DU-145 cells by confocal microscopy over 10 min (Fig. 1*C*). p53p-Ant-RhoB rapidly crossed the plasma membrane, with cytoplasmic, nuclear and nucleolar localization within 1 min, followed by more intense and diffuse accumulation. Similar results were detected in the PC-3 cells (data not shown).

Morphological Changes and Cell Viability in DU-145 Cells Treated with p53p-Ant—DU-145 cells were incubated with p53p-Ant, or Ant or p53p alone, or p53AntCONT peptides, and morphology was observed by phase contrast microscopy. Rapid and distinct morphological changes were observed (Fig. 2*A*) that were not seen in control Ant or p53p or p53AntCONT alone-treated cells. Loss of the typical cobblestone-like appearance was observed, with cells rounding and detaching from the plate at less than 1 h post-treatment. Both plasma and nuclear membranes became more distinct, associated with subsequent swelling. In contrast, PC-3 cells (null p53) showed an initial rounding and plasma membrane ruffling by 1 h, but then the great majority of PC-3 cells regained the appearance of untreated cells by 6 h with ~10% rounded and detached cells observed (Fig. 2*A*). As shown by MTT assay, p53p-Ant, but not

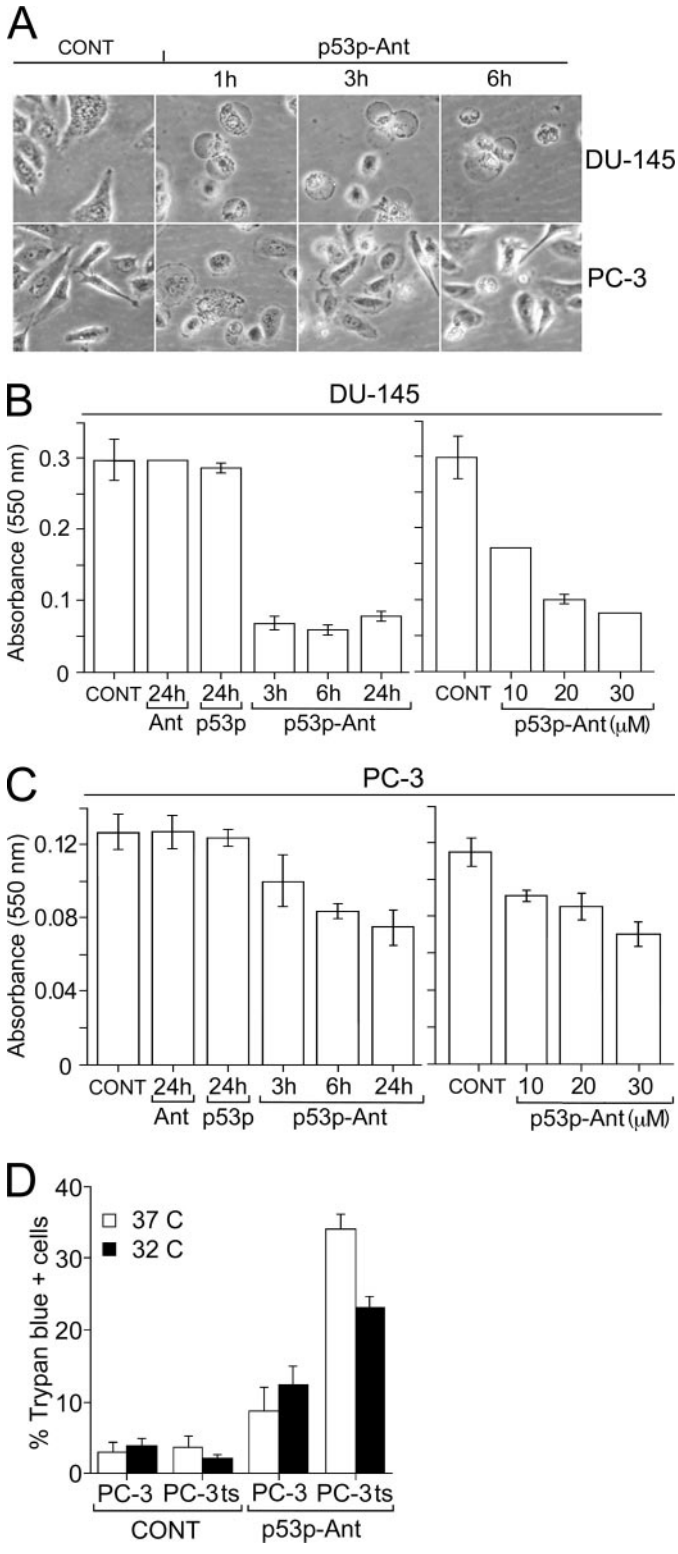

FIGURE 2. **Morphological changes and growth inhibition induced by p53p-Ant treatment.** *A*, DU-145 or PC-3 cells were untreated (*CONT*) or exposed to 30 μM p53p-Ant. The cells were photographed under phase contrast microscopy for up to 6 h. *B* and *C*, DU-145 (*B*) or PC-3 (*C*) cells were untreated (*CONT*) or exposed to 30 μM Ant, p53p, or p53p-Ant for 3 to 24 h or to 10, 20, or 30 μM p53p-Ant for 6 h. For *B* and *C*, cell viability was determined by MTT assay. The results represent mean absorbance ± S.D. ($n = 3$). *D*, trypan blue cell death in PC-3 cells or PC-3 stably transfected cells expressing a temperature-sensitive p53-143 at 37 °C (mutant p53) or 32 °C (wt p53) for 3 h. At least 200 cells were counted in triplicate.

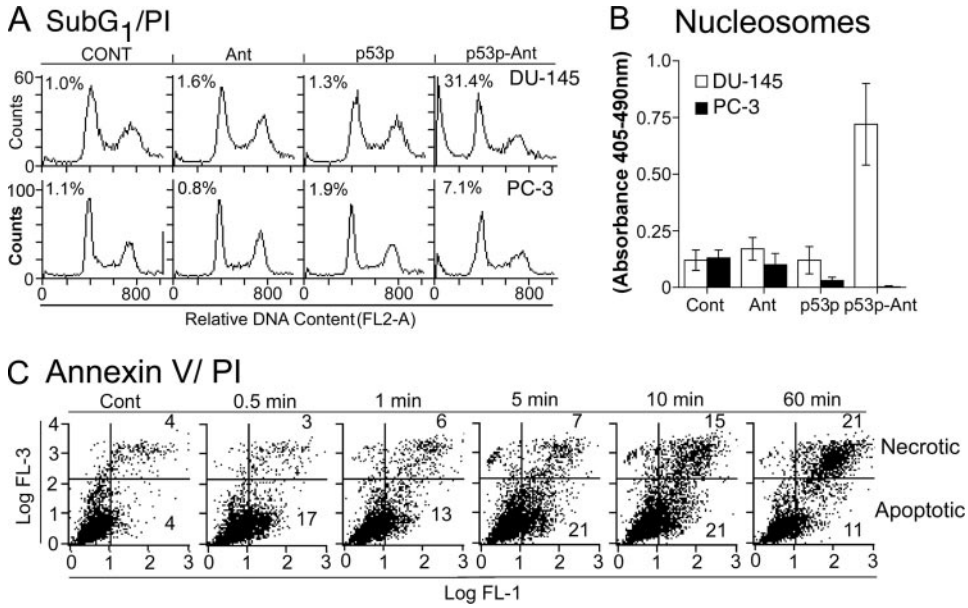

FIGURE 3. **Apoptotic markers in p53p-Ant-treated cells.** *A*, DU-145 or PC-3 cells ± 30 μM Ant, p53p, or p53p-Ant for 6 h. The cells were analyzed for PI-stained DNA content by flow cytometry. The percentage of cells with sub-G_1 DNA content are indicated. *B*, nucleosomes in cytoplasmic fractions of DU-145 and PC-3 lysates treated with Ant, p53p, or p53p-Ant peptides (Table 1) determined using an enzyme-linked immunosorbent assay. The results represent the mean absorbance ± S.D. ($n = 3$). *C*, Anx V and PI staining time course. DU-145 cells were exposed to 30 μM p53p-Ant for up to 1 h and analyzed by flow cytometry. Dot plots indicate PI-positive (necrotic) cells (FL-3) and Anx V-positive cells (FL-1). The percentage of cells in each quadrant is indicated.

the controls Ant or p53p alone, induced a reduction in viability as early as 3 h and up to 24 h after treatment (Fig. 2*B*). p53p-Ant was significantly more inhibitory to DU-145 than PC-3 cells at all time points tested. After 3 h, the PC-3 cells showed only a marginal toxicity of less than 8% compared with DU-145 cells, which exhibited more than 75% toxicity after the same treatment (Fig. 2*C*). The reduction in cell viability was concentration-dependent with an approximate IC_{50} of 30 μM, similar to the IC_{50} concentration previously found in breast cancer cells exposed to p53pAnt (Fig. 2*B*) (17). In contrast, concentrations up to 50 μM of control peptide p53-AntCONT did not show any inhibition of proliferation, in either PC-3 or DU-145 cells (data not shown).

Additional experiments found that 30 μM p53p-Ant increased the percentage of trypan blue-positive cells from 2.2 ± 0.6 to 31.5 ± 1.8% (14.3-fold) in DU-145 and 4.2 ± 1.0 to 8.9 ± 1.1% (2.1-fold) in PC-3 cells, consistent with the results from the viability assay and phase contrast microscopy. In addition, trypan blue-positive cells increased from 12.7 ± 0.7 to 20.5 ± 0.8% (1.6-fold) in the wt p53 prostate cancer cell line LNCaP; from 6.1 ± 2.2 to 10.7 ± 0.7% in the immortalized, nonmaligant prostate cell line P69; and from 5.3 ± 0.3 to 45.6 ± 3.1% (8.6-fold) and 7.2 ± 1.0 to 48.9 ± 2.3% (6.8-fold) in the mutant p53, prostate cancer cell lines 22R*v*1 and VCaP, respectively.

To further confirm that p53p-Ant-induced cell death was dependent on the presence of mutant p53, cell death in stably transfected temperature-sensitive PC-3 cells expressing mutant p53-143 at 37 °C and wild type p53 at 32 °C was determined. The cells were more sensitive to p53p-Ant at the mutant p53 temperature (37 °C) than at the wt p53 temperature (32°) (Fig. 2*D*). This is consistent with BIACORE data showing that p53p-Ant binds wt p53 with 100-fold lower affinity than mutant p53.

Measurement of Apoptotic Cell Death Induced by p53p-Ant—We reported that p53p-Ant induced apoptosis without necrosis in mutant p53 but not null p53 breast cancer cell lines (17). Therefore, we examined apoptotic markers in p53p-Ant-induced cytotoxicity. A concentration- and time-dependent sub-G_1 peak (typically 30–50%) was detected by flow cytometry of PI-stained cells but not with the controls Ant or p53p alone. Minor cytotoxicity of ~7% from p53p-Ant was observed in null p53 PC-3 cells (Fig. 3*A*). DU-145 cells showed a 5.7-fold increase nucleosomal DNA fragments (mono- and oligosomes) in cytoplasmic fractions after a 6-h exposure to p53p-Ant but not to Ant (1.4-fold) or p53p alone (0.9-fold) (Fig. 3*B*). In contrast, PC-3 cells did not show any accumulation of nucleosomal fragments after a 6-h exposure to p53p-Ant (Fig. 3*B*). When DU-145 cells were stained simultaneously with Anx V and PI, p53p-Ant induced an increase in Anx V+/PI− cells (apoptotic), within 0.5 min, which became Anx V+/PI+ cells (necrotic), after 5 min, indicating that p53p-Ant first induced apoptosis which was later switched to necrosis (Fig. 3*C*). In contrast, PC-3 cells, did not show significant cell death.

p53p-Ant-induced Death Is Independent of Fas and Caspase Activation—We reported that a 1-h exposure of breast cancer cells to p53p-Ant increased Fas expression without mRNA or protein synthesis, activation of caspase-8 and 3, and PARP cleavage (17). Therefore, we investigated whether prostate cancer cell death by p53p-Ant also involved Fas and caspase activation. Treatment with p53p-Ant for 1 h failed to increase Fas membrane expression by fluorescence-activated cell sorter analysis (Fig. 4*A*). However, the same treatment increased Fas expression in mutant p53 MDA-468 human breast cancer cells, consistent with our previous findings (17). The PARP cleavage product was also not observed in DU-145 cells under conditions of maximal cell death by peptide. However, DU-145 cells treated with 50 nM PAC induced classical apoptosis (21) with PARP cleavage (Fig. 4, *B* and *C*). This demonstrated that under conditions that induced apoptosis (PAC treatment), PARP cleavage does occur in DU-145 cells. Additionally, PAC, but not p53p-Ant, increased caspase-3 and -8 activities in DU-145 cells. The lack of caspase-3 activation from p53p-Ant was confirmed in low passage DU-145 cells from ATCC. In addition, pretreatment of DU-145 cells with the pan-caspase inhibitor, BOC-Asp-FMK, significantly blocked the apoptotic effects of PAC (sub G_1 fraction), but not the p53p-Ant-induced sub-G_1 frac-

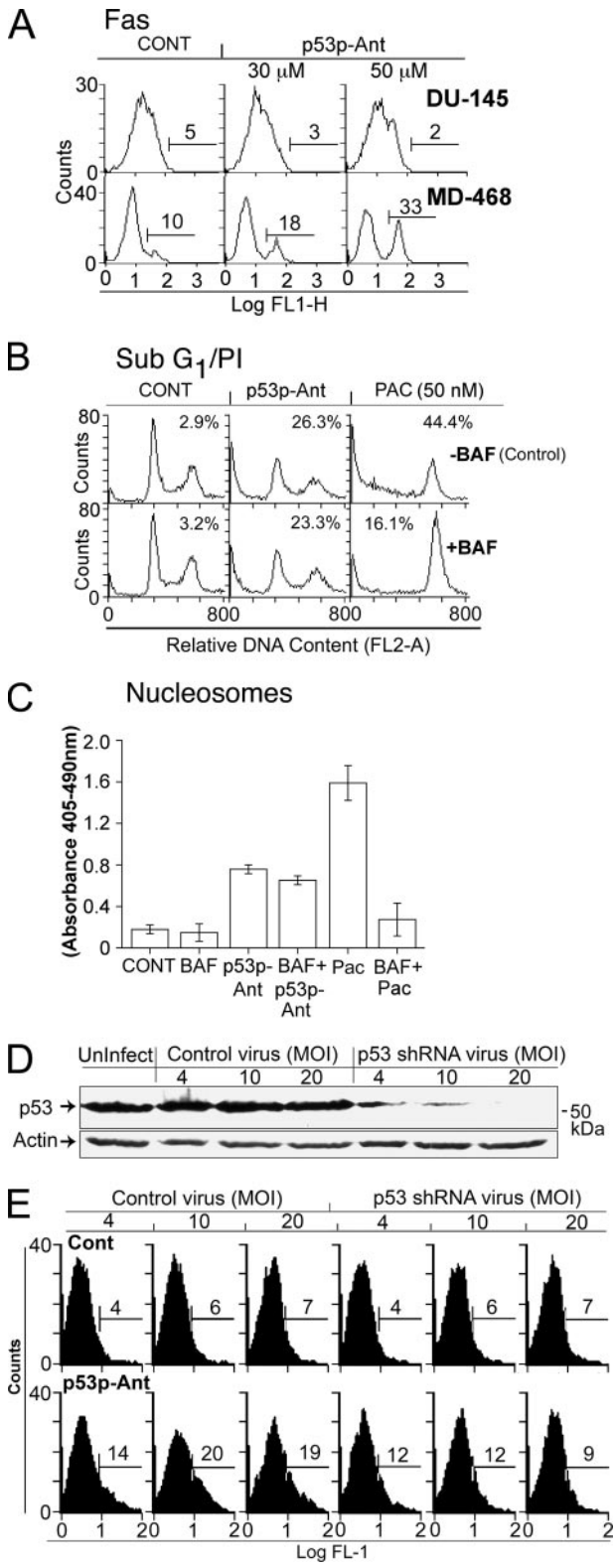

FIGURE 4. **Apoptosis in p53p-Ant-induced DU-145 cell death.** *A*, Fas expression changes from p53p-Ant in DU-145 cells or MD-468 breast cancer cells ± 30 or 50 μM p53p-Ant for 1 h. The results are expressed as fluorescent intensity of 5000 cells. *B*, DU-145 cells were untreated (−) or preincubated (+) with the pan caspase inhibitor, BOC-Asp-FMK (*BAF*) (50 μM for 20 min) and then untreated or exposed to 30 μM p53p-Ant for 6 h. The cells were analyzed for PI-stained DNA. The values indicate the percentages of cells with sub-G_1 DNA content. *C*, DU-145 cells were treated as in *B*. Nucleosomes in cytoplasmic fractions of cell lysates were determined using an enzyme-linked immunosorbent assay. The results represent the mean absorbance ± S.D. ($n = 3$). PAC treatment (50 nM, 48 h). *D*, Western analysis of p53 expression in DU-145 cells using anti-p53 DO-1 antibody (epitope 11–25 aa) after pAd/U6/p53-shRNA (p53 shRNA) or pAd/U6/shuffled-p53-shRNA treatment (66 h) done from parallel plates at the same time as Anx V staining in *E*. *MOI*, multiplicity of infection (number of adenovirions/number of cells present). *E*, Anx V staining of pAd/U6/p53-shRNA (p53 shRNA) *versus* pAd/U6/shuffled-p53-shRNA ± 6 h treatment with 30 μM p53p-Ant.

tion (Fig. 4*B*) and nucleosomes (Fig. 4*C*). There was no change in the basal levels of Bax, Bcl-2, Bak, or PUMA in Westerns from p53p-Ant exposure to DU-145 cells (data not shown).

To determine whether the p53p-Ant-induced cell death in DU-145 cells was dependent on p53 as in breast cancer cells, DU-145 cells were treated with adenovirus-containing shRNA against p53 or an adenovirus containing the same nucleotides in a shuffled sequence. After treatment with shRNA (multiplicity of infection of 20) containing adenovirus, p53 expression was reduced by >90% as determined by Western blot (Fig. 4*D*). Resistance to cell death-induced p53p-Ant increased in p53-shRNA adenovirus-infected cells compared with cells treated with the shuffled sequence (Fig. 4*E*), which corresponded to the level of adenovirus treatment and the level of p53 (Fig. 4*D*). Thus, p53p-Ant-induced death in DU-145 cells did not involve the extrinsic (FAS, caspase-8) or intrinsic pathways (Bcl-2, Bax, Bak, PUMA, or caspase-3), yet the majority of cell death was p53-dependent.

Involvement of Necrosis in p53p-Ant-induced Death of DU-145 Cells—Because p53p-Ant-induced cell death in DU-145 cells was associated with incomplete features of apoptosis, we investigated other mechanisms of cell death. Extracellular LDH release doubled after a 10-min exposure to p53pAnt and continued to increase over time (Fig. 5*A*). The release of LDH in response to p53p-Ant was confirmed in low passage DU-145 cells. Fluorescence microscopy showed an increase in the percentage of ethidium homodimer-stained cells after 10 min, indicative of a porous or damaged plasma membrane. These results were quantitated, showing a similar slope pattern analogous to the curve for LDH release (Fig. 5*B*).

Intracellular energy levels (ATP) dissipate early and rapidly in cells undergoing necrosis but not in apoptosis (10). Therefore, intracellular ATP levels were assessed after peptide treatment. ATP levels decreased 63% from initial baseline levels after 30 min but started as early as 5–10 min after peptide exposure with a 43% decrease in ATP levels (Fig. 5*C*). The ATP decline was not affected by the PARP inhibitor, 3-aminobenzamide (Fig. 5*D*). Electron microscopy showed a mixture of necrotic and apoptotic cells, with a higher proportion of necrotic cells at 30 min, characterized by swollen cellular size and lower cytoplasmic density (Fig. 6*A*). Analysis at 30 min and 1 h showed definite broken plasma membranes, which were consistent with a necrotic form of cell death (Fig. 6*B*). At 3 and 6 h after peptide exposure, cells showing apoptotic features were observed, characterized by high cytoplasmic density and condensed, pyknotic DNA (Fig. 6*A*). Together, the LDH release and decrease of intracellular ATP with the ethidium homodimer fluorescence and electron microscopic studies suggested that many DU-145 cells showed features of necrosis by 10 min and other cells developed apoptosis at 0.5 min (Anx +/PI−) and

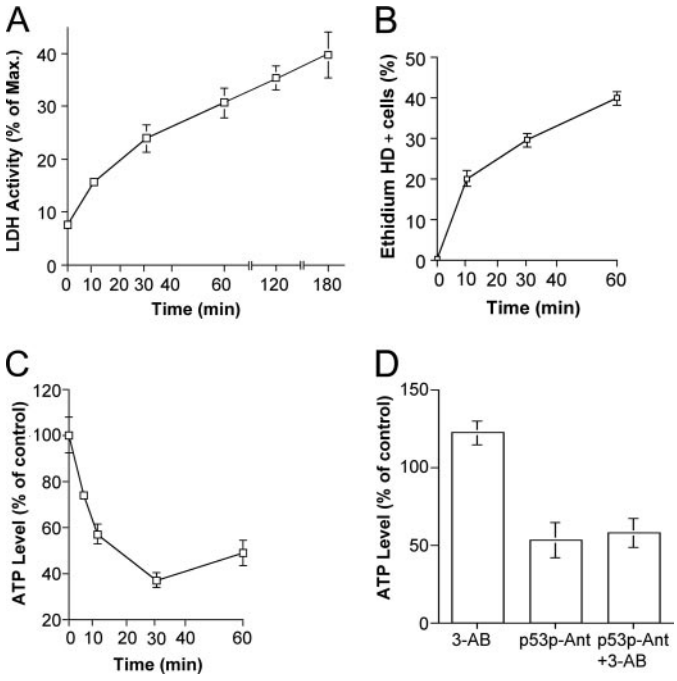

FIGURE 5. **Necrosis in p53p-Ant-induced DU-145 cell death.** *A*, LDH release time course. ±30 μM p53p-Ant. The results are expressed as percentages of the maximum LDH release ("Experimental Procedures") and represent the mean absorbance ± S.D. ($n = 3$). *B*, cell fluorescence time course. The cells were cultured on poly-D-lysine-coated coverslips ± 30 μM p53p-Ant and stained with Calcein AM and ethidium homodimer-1. Green fluorescent cells (living) and red fluorescent cells (with damaged plasma membranes) were quantitated and expressed as a percentage. The results represent the mean number of ethidium homodimer-positive cells ± S.D. ($n = 3$, 300 cells/point). *C*, intracellular ATP time course; cells ± 30 μM p53p-Ant. ATP levels were determined on a TD 20/20 luminometer at 560 nm. The results are expressed as percentages of untreated controls and represent mean luminosity ± S.D. ($n = 3$). *D*, ATP analysis as in *C*. The cells were preincubated with 3-aminobenzamide (*3-AB*, 10 mM) for 30 min followed by incubation with 30 μM p53p-Ant ± 3-aminobenzamide for 10 min. The results are expressed as percentages of untreated controls and represent the mean luminosity ± S.D. ($n = 3$).

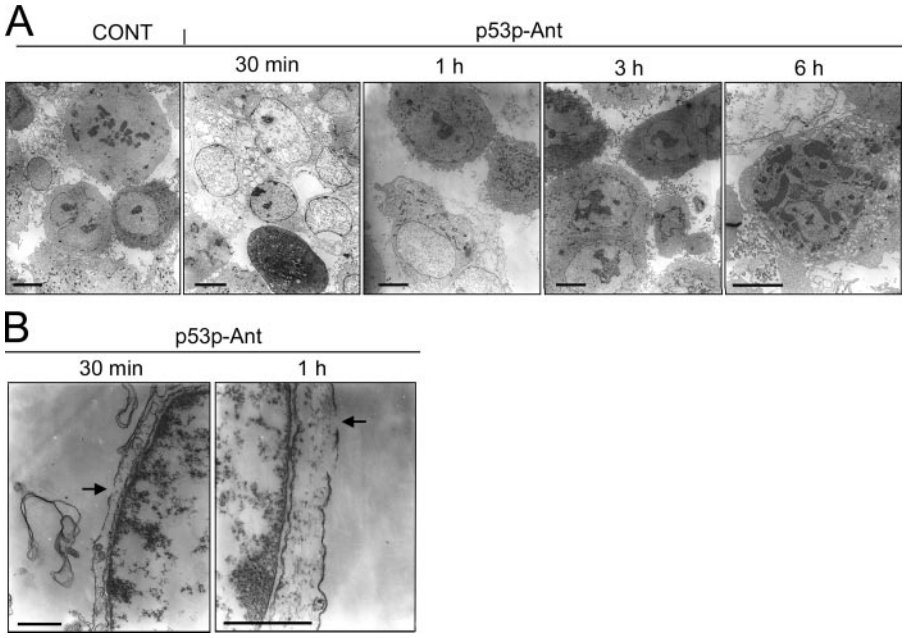

FIGURE 6. **Electron microscopy of p53p-Ant-treated DU-145 cells.** *A*, DU-145 cells were untreated or exposed to 30 μM p53p-Ant for the times indicated. Representative photomicrographs are shown for each time point. *Bars*, 5 μm. *B*, higher magnifications of the plasma membrane of DU-145 cells after p53p-Ant treatment for the indicated times. The *arrows* indicate breaks in the plasma membrane. Bars = 0.5 μm. *CONT*, control.

then apoptotic features at later time points. This is consistent with the annexin V/PI studies showing that necrotic cells appeared between 5 and 10 min but with an earlier apoptotic population (annexin V+/PI−) at 0.5 min and persisting up to and after 60 min (Fig. 3*C*). Thus, the majority of cell death in DU-145 cells by p53p-Ant begins as apoptotic after 0.5 min, which is converted to necrosis after ~10 min. However, not all cells are converted to necrosis, and some develop an apoptotic morphology after 3 h.

Involvement of ROS in p53p-Ant-induced Death—The drop in ATP levels suggested that mitochondrial disruption may be an important event in the early stages of death induced by p53p-Ant in mutant p53 prostate cancer cells. ROS production from p53p-Ant treatment was assessed using DCFDA and DHE. DCFDA detects general ROS and DHE is somewhat specific for O_2^- (22). Cells treated with p53p-Ant demonstrated a 9-fold increase in DHE fluorescence (Fig. 7*A*) and a 5.4-fold increase in DCFDA fluorescence (not shown) within 1 h. The increase in DHE fluorescence was peptide dose-dependent (Fig. 7*B*) and not seen in PC-3 cells (Fig. 7*C*). The O_2^- scavenger, Tiron and the superoxide dismutase mimetic MnTMPyP partially reversed the p53p-Ant-induced DHE fluorescence (Fig. 7*D*), as well as p53p-Ant-induced cell death (Fig. 7*E*). In contrast, *N*-acetylcysteine did not have any effect on p53p-Ant-induced death (Fig. 7*E*). *N*-Acetylcysteine mainly quenches H_2O_2 and not O_2^-. In an attempt to elucidate why the mutant p53 prostate cancer cells underwent necrosis and the mutant p53 breast cancer cells undergo apoptosis from p53p-Ant exposure, O_2^- levels were assessed. Mutant p53 human breast MD-468 cells showed a 2.3-fold increase in O_2^- levels compared with 4.7-fold in prostate DU-145 cells under conditions that induce apoptosis and necrosis, respectively (Fig. 7*F*). Further examination of O_2^- accumulation over time indicated that O_2^- increased as early as 1 min after exposure to p53p-Ant and corresponded closely with increased Anx V+/PI− cells until after a 5-min exposure to p53p-Ant (Fig. 7*G*). In addition, TUNEL+ cells increased after the rise in Anx V+/PI− (apoptotic) cells, and after 5 min, Anx V+/PI+ (necrotic) cells began to accumulate with fewer Anx V+/PI− (apoptotic) cells observed (Fig. 7*H*). We found that O_2^- accumulation and Anx V+ cells were blocked by pretreatment with 5 mM KCN, suggesting that mitochondria were the source of O_2^- accumulation in response to p53p-Ant (Fig. 7*I*).

These results suggested that the mechanism of p53p-Ant cell death in mutant p53 DU-145 cells may be mediated by mitochondrial ROS in the form of O_2^-, and p53p-Ant initially produced apoptosis, which was converted to necrosis when O_2^- accumulation reached a critical level.

p53p-Ant-induced Targeted Necrosis in Drug-resistant DU-145 Cell Lines—We investigated whether the p53p-Ant-mediated necrosis in DU-145 cells may circumvent resistance to chemotherapy-induced apoptosis. The DURC-1 cell line, derived from parental DU-145 cells, were resistant to topotecan and camptothecin as described under "Experimental Procedures" (19). The DU-TaxR cell line are parental DU-145 cells made resistant to PAC by continuous exposure in our laboratory. By TUNEL analysis, DU-145 parental cells were sensitive, and DURC-1 and DU-TaxR cells were resistant to topotecan (1.0 μM; Fig. 8*A*) and PAC (10 nM; Fig. 8*B*), respectively. However, DURC-1 and DU-TaxR cells were equally sensitive as DU-145 parental cells to p53p-Ant (Fig. 8*C*). Similar results were obtained for these lines in PI and trypan blue assays (data not shown). DURC-1 and DU-TaxR cells, exposed to p53p-Ant, showed characteristics of necrosis as indicated by rapid LDH release (1 h) and rapid decline in intracellular ATP (1 h; Fig. 8, *D* and *E*), respectively.

DISCUSSION

This study sought to investigate whether p53p-Ant could induce alternative cell death pathways in mutant p53 prostate cancer cells and whether this switch could overcome apoptotic resistance. This strategy is of particular interest in prostate cancer, because resistance to chemotherapy almost always develops *in vivo* during treatment of metastatic hormone-independent disease (23, 24).

Our lab and others have shown that the C-terminal p53-derived peptide p53p-Ant induced selective and rapid apoptosis in tumor cells that was directly correlated with levels of mutant p53 while nontoxic to nonmalignant or normal cells with normal levels of wt p53 (15, 17). Also, p53p-Ant was nontoxic to null p53 breast cancer lines (MDA-MB-157), nonmalignant breast lines with wt p53 (MCF10-2A), a normal skin fibroblast line (27sk), (17), and normal human peripheral blood

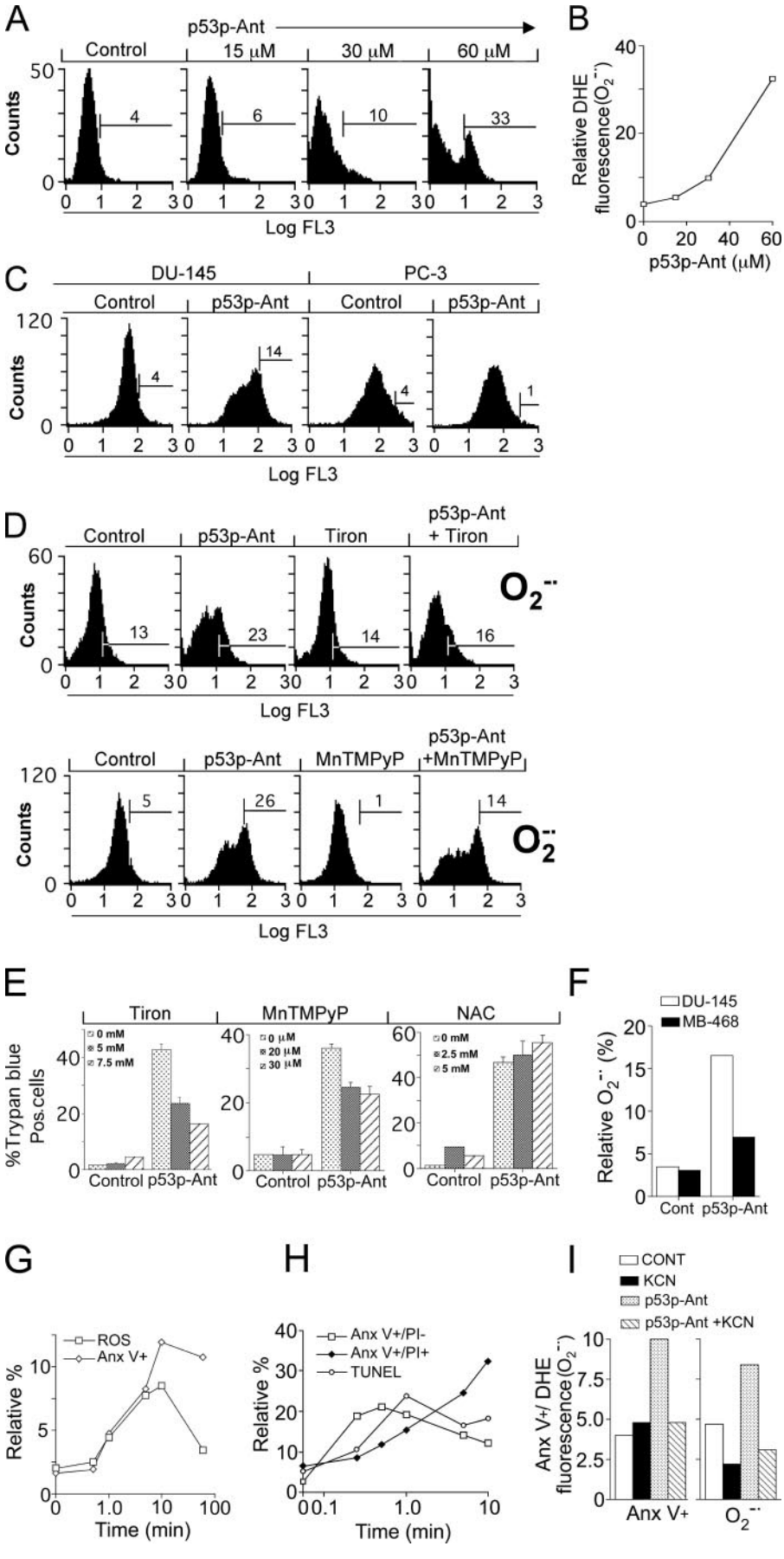

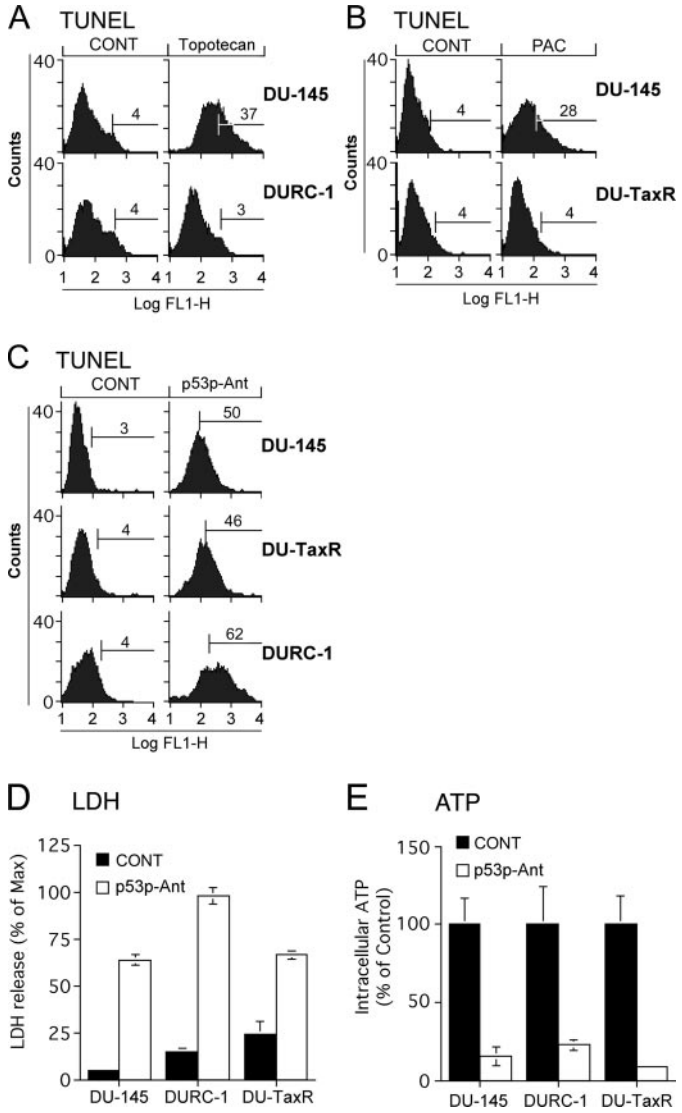

FIGURE 8. **Effect of p53p-Ant in DU-145 drug-resistant cells.** *A–C*, TUNEL analysis in DU-145, DURC-1 or DU-TaxR cells exposed for 48 h to indicated concentrations of topotecan (*A*), PAC (*B*), 30 μM p53p-Ant (3 h) (*C*). The percentage of particles gated is shown. *D*, LDH release in DU-145, DURC-1, or DU-TaxR cells exposed to 30 μM p53p-Ant for 1 h (see Fig. 5*A*). *E*, Intracellular ATP levels in DU-145, DURC-1, or DU-TaxR cells exposed to 30 μM p53p-Ant for 1 h (see Fig. 5*C*). The experiments were performed three times, and the means ± S.D. are shown.

CD34-positive stem cell progenitors for CFU-GEMM (25) that express low levels of wt p53. Surface plasma resonance data (Biacore) suggested that p53p-Ant bound both purified mutant and wt p53 with $>10^2$-fold increased binding affinity constants for mutant p53, compared with wt p53.[3] Mechanistically, p53p-Ant binds to mutant p53, which alters its three-dimensional conformation restoring partial wt p53 functional activity for nontranslational/nontranscriptional Fas-mediated apoptosis (17, 18). Studies in our lab suggest that the binding site for the peptide is the p53 tetramerization domain of p53 (aa 326–353).[3]

In this study, we have investigated the effects of p53p-Ant in nine prostate cell lines concentrating on mutant p53 (DU-145 cells) or null p53 (PC-3 cells). In DU-145, but not PC-3 cells, p53p-Ant induced rapid morphological and biochemical changes typical of necrosis. Anx V/PI studies at early time points (0.5 min) showed that there was an initial increase in Anx V+/PI− (apoptotic) cells, many of which became rapidly necrotic starting after ~10 min. Electron microscopy studies found the presence of both apoptotic and necrotic cells, with a greater proportion of necrotic cells after 30 min. This is consistent with many cells switching to the necrotic pathway within 30 min and not having enough time to develop an apoptotic morphology. Cells that did not switch to the necrotic pathway developed an apoptotic morphology consisting of high cytoplasmic density and condensed pyknotic DNA, which was observed after 3 or 6 h (17). Also, the p53-null PC-3 cells were relatively resistant to the effects of p53p-Ant, and p53-shRNA reversed p53p-Ant-induced Anx V+ cells, suggesting that both apoptosis and necrosis were p53-dependent.

In previous results, the apoptosis in breast cancer cell lines was associated with increased extracellular expression of Fas, activation of caspase-8, and cleavage of PARP. No significant expression changes were seen in apoptotic regulators such as Bax, Bak, Bcl-XL, and PUMA, suggesting that the extrinsic pathway but not the intrinsic pathway was involved in p53p-Ant-induced death in breast cancer cells. Similarly, p53p-Ant-treated DU-145 cells did not demonstrate changes in Bcl-2 family members, but in contrast (17), Fas and caspase activation were absent, and the pan caspase inhibitor BOC-Asp-FMK did not inhibit p53p-Ant-mediated death. The data suggest that in DU-145 cells, p53p-Ant activated neither the intrinsic or extrinsic pathways for apoptosis to detectable levels.

Some apoptotic pathways do not require the action of caspases. For example, p53-dependent radiation-induced neuronal cell death was not blocked by caspase inhibitors (26). ROS may induce a caspase-independent form of apoptosis, possibly because caspases can be inhibited by a high oxidizing environment. We found that p53p-Ant increased ROS in DU-145 cells, but not in PC-3 cells. *N*-Acetylcysteine, which is not a direct O_2^- scavenger (27), had no effect on p53p-Ant-induced cell death, but the O_2^- scavenger Tiron and superoxide dismutase mimetic MnTMPyP partially abrogated cell death, suggesting that O_2^- was responsible for inducing caspase-independent apoptosis in mutant p53 DU-145 cancer cells. However, we cannot yet exclude the role of novel, as yet undiscovered

[3] Y. Li, R. Rosal, Y. Mao, P. Brandt-Rauf, and R. L. Fine, unpublished data.

FIGURE 7. **O_2^- levels in p53p-Ant-induced DU-145 cells.** *A*, DU-145 cells ± increasing concentrations of p53p-Ant for 1 h. DHE was added to the cell culture in the last 30 min of incubation. The values indicate the relative percentage of cells demonstrating DHE fluorescence (superoxide accumulation). *B*, plot of data in *A*. *C*, DU-145 or PC-3 cells were treated with or without 60 μM p53p-Ant for 1 h and DHE (O_2^- levels) fluorescence determined. *D*, cells were preincubated for 30 min with either Tiron (5 mM) or MnTMPyP (30 μM) prior to p53p-Ant (60 μM) for 1 h and DHE fluorescence was analyzed as in *A*. *E*, trypan blue analysis of DU-145 cells treated as in *D*. At least 600 cells were counted per sample. All of the experiments were repeated. *F*, DHE fluorescence of DU-145 *versus* MD-468 after 5 min of incubation with p53p-Ant under conditions that induce necrosis and apoptosis, respectively. *G*, DHE fluorescence and Anx V+ time course in DU-145 cells. *H*, time course of apoptotic cells (Anx V+/PI−) and necrotic cells (Anx V+/PI+) and TUNEL-positive cells. *I*, Anx V+ and DHE fluorescence after 5 min ± 30 μM p53p-Ant ± 5 mM KCN. *Cont*, control.

caspases, which were not inhibited by BOC-Asp-FMK or ROS and that are independent of the Fas and Bcl-2 family pathways in the mechanism of p53p-Ant-mediated apoptosis in DU-145 cells (28). Alternatively, expression of inhibitory protein(s) at the apex of the caspase activation cascade that prevent activation of caspase-8 may occur (29, 30). An example of this is the action of overexpressed c-FLIP, which inhibits caspase-8 activation. However, we found no evidence of c-FLIP overexpression in DU-145 cells by Western blot (data not shown).

One explanation for necrosis induction may be an incomplete execution of the mechanisms of apoptosis as a consequence of a limited supply of intracellular ATP (9). The aborted mechanisms of apoptosis may explain why some features of apoptosis were detected without signs of classical apoptosis in the intrinsic or extrinsic pathways. Anx V+/PI− (apoptotic) in DU-145 cells were observed within 0.5 min, and necrosis (Anx V+/PI+) occurred within 10 min after the addition of peptide (Figs. 3*C* and 5, *A* and *B*). The ATP levels in DU-145 cells dropped precipitously within 10 min after peptide exposure (43–63%), and PARP was not inactivated. However, incubation with the PARP inhibitor 3-aminobenzamide did not block the ATP decline in peptide-treated DU-145 cells, suggesting that continued PARP activity was not responsible for the decline in ATP (Fig. 5*D*). Another explanation for necrosis is that the ATP loss occurred from plasma membrane rupture. p53p-Ant was found to induce rapid membrane ruffling in both DU-145 and PC-3 cells, and it has been predicted that Antennapedia is internalized by a penetration mechanism (31). Thus, necrosis could be from entry of the peptide through the plasma membrane. However, contrary to this idea, both prostate cancer lines displayed rapid and equal penetration of Ant-p53p-RhoD into all cellular compartments, yet only the DU-145 cells underwent cell death, whereas the PC-3 cells recovered and showed only 8–10% cytotoxicity with no decrease in ATP levels. In addition, Ant alone, and the control peptide p53-AntCONT, which penetrated membranes, did not produce significant ATP or LDH loss or cytotoxicity. We have found in other studies that Ant with p53p produced a hydrophobic structure with a high density of positive charges from the multiple basic, positively charged aa residues that, when passing through the plasma membrane, caused a transient loss of integrity and nonapoptotic death in a minority of cells (<10%) (32). However, Tiron, an O_2^- scavenger, and the superoxide dismutase mimetic MnTMPyP partially abrogated p53p-Ant-induced cell death. Because these inhibitors are unlikely to block penetration of p53p-Ant, this result argues that O_2^- accumulation may be important for the mechanism of necrosis induced by p53p-Ant. Necrosis was found to occur at the peak of O_2^- accumulation (10 min) in our study. Other studies have proposed that ROS at low concentrations trigger apoptosis but at higher concentrations trigger necrosis (33).

Some studies have found ROS to be downstream mediators of wt-p53-dependent apoptosis (34), suggesting that functional p53 can regulate the intracellular redox state for induction of apoptosis. This regulatory function of p53 may explain our previous findings where p53p-Ant restored partial functional activity to mutant p53 (17) and the involvement of O_2^- in p53p-Ant-induced necrosis. We hypothesize that p53p-Ant may be restoring partial wt p53 activity to mutant p53 in multiple prostate cancer cell lines. This functional, mutant p53 may induce O_2^- formation and subsequent cell death. The findings that ROS is not formed in null p53 PC-3 and that this cell death is caspase-independent are consistent with this model. ROS has been found to induce a form of cell death lacking features of classical caspase-dependent apoptosis (35, 36).

However, ROS has also been found to trigger classical apoptosis (37, 38) or necrosis, dependent upon its levels (33). We have found that p53p-Ant induced a lower level of ROS in mutant p53 breast cancer cells (MDA-468), which undergo only extrinsic (Fas-mediated) apoptosis from p53p-Ant (data not shown). However, the level of induction of ROS may not totally explain why DU-145 cells are directed more into necrosis and breast cancer cells are directed more into apoptosis from p53p-Ant. As we found, p53p-Ant may induce different levels of ROS in different cell types. In addition, different cell types may be more or less sensitive to different levels of ROS because of intrinsic differences in levels of free-radical scavengers. In addition, the basal level of ATP or recovery of ATP levels may be an important determinant for apoptosis *versus* necrosis. In fact, p53p-Ant exposure in MB-468 breast cancer cells produced a 42% decline in intracellular ATP but recovered to basal ATP levels after 4 h, whereas p53p-Ant exposure to DU-145 cells produced a 67% decline, which did not recover to basal levels after 4 h.[4] This lack of ATP recovery may be vital for the commitment to necrosis. This may also explain the mixture of necrotic and apoptotic DU-145 cells that were observed. Within the DU-145 cell population there may be cells that have a higher or lower sensitivity to ROS levels because of differences in free radical scavengers and/or basal ATP levels, driving some toward apoptosis and some toward necrosis. However, the major difference between DU-145 and PC-3 cells is the null p53 status; thus, the target for p53p-Ant is missing and explains the lack of cell death, ATP decline, and ROS accumulation in PC-3 cells.

Importantly, this report is the first to show that peptide-mediated restoration of wt function to mutant p53 in cells can cause necrosis, suggesting that wt p53 may induce necrosis, as well as apoptosis, but associated with differential levels of ROS (*i.e.* low O_2^-, apoptosis high; O_2^-, necrosis from loss of ATP).

The induction of targeted necrosis in our model can bypass apoptotic resistance. Two DU-145 cell lines made resistant to topotecan or PAC-induced apoptosis retained sensitivity to p53p-Ant. This suggests that p53p-Ant has the potential for circumventing resistance to classical apoptosis by eliciting targeted necrosis. In addition, targeted necrosis induced by p53p-Ant is specific to cells expressing mutant p53, which may obviate the major problem in utilizing the necrotic death pathway in cancer therapy, namely its inflammatory reaction and lack of specificity for cancer and normal cells. Thus, targeted necrosis by p53 peptide can potentially retain the specificity of apoptosis for mutant p53 tumor cells and bypass resistance mechanisms for apoptosis. The determinant for whether a

[4] R. D. Dinnen and R. L. Fine, unpublished data.

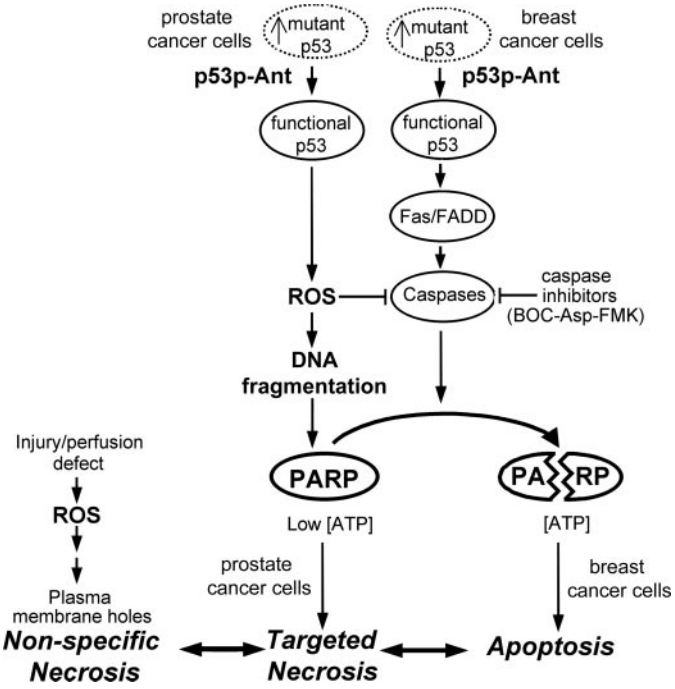

FIGURE 9. **Pathways of nonspecific necrosis, targeted necrosis, and apoptosis.** Wild type p53, through the action of ROS, Fas, or Bcl-2 family of proteins, activates caspases, resulting in apoptosis. Necrosis is activated by injury or perfusion defects, leading to generation of ROS. Alternatively, p53p-Ant preferentially binds to mutant p53 and alters its conformation resulting in functional p53. The functional mutant p53 may mediate generation of ROS leading to DNA nicks, nucleosomal degradation, and mitochondrial membrane damage with loss of ATP pools but without caspase-3 activation. This leads to targeted necrosis because it will only be activated in mutant p53 cancer cells, which express sufficient threshold p53 target for the peptide and decreased ATP, which commits the cell to undergo necrosis. Alternatively, functional p53 may act via the Fas/FADD pathway leading to apoptosis, as in breast cancer cells, which do not undergo massive loss of ATP.

cell undergoes apoptosis or targeted necrosis may depend upon its ability to recover ATP levels before there is an irreversible commitment to necrosis. This, at least in our cell model, seems to occur at ~10 min. Thus, this report adds to the previous report by Ha and Snyder (13) demonstrating that the "switch" point for turning apoptosis into necrosis was through inhibition of PARP cleavage, which lowered ATP pools. In our study the increased ROS O_2^- levels induced mitochondrial damage, causing a precipitous drop in ATP pools inducing the switch from apoptosis to necrosis. Thus, caspase inhibition and O_2^- can lead to lower ATP pools, inducing the switch.

In conclusion, this study demonstrated that p53p-Ant induced significant cell death only in mutant p53 prostate cancer cells, in a p53-dependent and caspase-independent manner via ROS-associated loss of mitochondrial ATP. The form of cell death may be dependent upon the cell type and suggests the possibility of an unknown pathway leading to activation of targeted necrosis (Fig. 9). These data also implicate a possible role for functional mutant or wt p53 in the death pathway of necrosis. Because p53p-Ant can induce multiple mechanisms of cell death dependent on cell type, it may provide an interesting tool to investigate the mechanisms of targeted necrosis and the switch from apoptosis to necrosis. If this switch can be definitively identified, it may become possible to induce targeted necrosis in cancer cells resistant to apoptosis. One possible way to regulate this decision point is by generating high levels of ROS (O_2^-) and modulating ATP pools or their recovery so that the cell is committed to necrosis after exposure to an inducer of apoptosis.

Acknowledgments—We thank Panayotis Pantazis of the University of Miami for generously supplying the DURC-1 cell line and Dr. Paul Fisher and Anthony Raffo for the helpful discussions.

REFERENCES

1. Raffo, A. J., Perlman, H., Chen, M. W., Day, M. L., Streitman, J. S., and Buttyan, R. (1995) *Cancer Res.* **55,** 4438–4445
2. Isaacs, W. B., Carter, B. S., and Ewing, C. M. (1991) *Cancer Res.* **51,** 4716–4720
3. Effert, P. J., Neubauer, A., Walther, P. J., and Liu, E. T. (1992) *J. Urol.* **147,** 789–793
4. Wang, L. G., Ossowski, L., and Ferrari, A. C. (2001) *Cancer Res.* **61,** 7544–7551
5. Miyake, H., Hara, I., Kamidono, S., Gleave, M. E., and Eto, H. (2003) *Oncol. Rep.* **10,** 469–473
6. Chen, M. W., Vacherot, F., De La Taille, A., Gil-Diez-De-Medina, S., Shen, R., Friedman, R. A., Burchardt, M., Chopin, D. K., and Buttyan, R. (2002) *Oncogene* **21,** 7861–7871
7. Howell, S. B. (2000) *Mol. Urol.* **4,** 225–231
8. Do, T. N., Rosal, R. V., Drew, L., Raffo, A. J., Michl, J., Pincus, M. R., Friedman, F. K., Petrylak, D. P., Cassai, N., Szmulewicz, J., Sidhu, G., Fine, R. L., and Brandt-Rauf, P. W. (2003) *Oncogene* **22,** 1431–1444
9. Formigli, L., Papucci, L., Tani, A., Schiavone, N., Tempestini, A., Orlandini, G. E., Capaccioli, S., and Orlandini, S. Z. (2000) *J. Cell. Physiol.* **182,** 41–49
10. Leist, M., Single, B., Castoldi, A. F., Kuhnle, S., and Nicotera, P. (1997) *J. Exp. Med.* **185,** 1481–1486
11. Bonfoco, E., Krainc, D., Ankarcrona, M., Nicotera, P., and Lipton, S. A. (1995) *Proc. Natl Acad. Sci. U. S. A.* **92,** 7162–7166
12. Eguchi, Y., Shimizu, S., and Tsujimoto, Y. (1997) *Cancer Res.* **57,** 1835–1840
13. Ha, H. C., and Snyder, S. H. (1999) *Proc. Natl Acad. Sci. U. S. A.* **96,** 13978–13982
14. Prabhakaran, K., Li, L., Borowitz, J. L., and Isom, G. E. (2004) *Toxicol. App. Pharmacol.* **195,** 194–202
15. Selivanova, G., Iotsova, V., Okan, I., Fritsche, M., Strom, M., Groner, B., Grafstrom, R. C., and Wiman, K. G. (1997) *Nat. Med.* **3,** 632–638
16. Selivanova, G., Ryabchenko, L., Jansson, E., Iotsova, V., and Wiman, K. G. (1999) *Mol. Cell. Biol.* **19,** 3395–3402
17. Kim, A. L., Raffo, A. J., Brandt-Rauf, P. W., Pincus, M. R., Monaco, R., Abarzua, P., and Fine, R. L. (1999) *J. Biol. Chem.* **274,** 34924–34931
18. Li, Y., Mao, Y., Rosal, R. V., Dinnen, R. D., Williams, A. C., Brandt-Rauf, P. W., and Fine, R. L. (2005) *Int. J. Cancer* **15,** 55–64
19. Urasaki, Y., Laco, G. S., Pourquier, P., Takebayashi, Y., Kohlhagen, G., Gioffre, C., Zhang, H., Chatterjee, D., Pantazis, P., and Pommier, Y. (2001) *Cancer Res.* **61,** 1964–1969
20. Schomber, T., Kalberer, C. P., Wodnar-Filipowicz, A., and Skoda, R. C. (2004) *Blood* **103,** 4511–4513
21. Haldar, S., Chintapalli, J., and Croce, C. M. (1996) *Cancer Res.* **56,** 1253–1255
22. Halliwell, B., and Whiteman, M. (2004) *Br. J. Pharmacol.* **142,** 231–255
23. DiPaola, R. S., and Aisner, J. (1999) *Semin. Oncol.* **26,** 112–116
24. MacGrogan, D., and Bookstein, R. (1997) *Semin. Cancer Biol.* **8,** 11–19
25. Senatus, P. B., Li, Y., Mandigo, C., Nichols, G., Moise, G., Mao, Y., Brown, M. D., Anderson, R. C., Parsa, A. T., Brandt-Rauf, P. W., Bruce, J. N., and Fine, R. L. (2005) *Mol. Cancer Ther.* **5,** 20–28
26. Johnson, M. D., Xiang, H., London, S., Kinoshita, Y., Knudson, M., Mayberg, M., Korsmeyer, S. J., and Morrison, R. S. (1998) *J. Neurosci. Res.* **54,** 721–733

27. Aruoma, O. I., Halliwell, B., Hoey, B. M., and Butler, J. (1989) *Free Radic. Biol. Med.* **6,** 593–597
28. Sperandio, S., de Belle, I., and Bredesen, D. E. (2000) *Proc. Natl Acad. Sci. U. S. A.* **97,** 14376–14381
29. Rokhlin, O. W., Glover, R. A., and Cohen, M. B. (1998) *Cancer Res.* **58,** 5870–5875
30. Hyer, M. L., Sudarshan, S., Kim, Y., Reed, J. C., Dong, J. Y., Schwartz, D. A., and Norris, J. S. (2002) *Cancer Biol. Ther.* **1,** 401–406
31. Derossi, D., Chassaing, G., and Prochiantz, A. (1998) *Trends Cell Biol.* **8,** 84–87
32. Li, Y., Rosal, R. V., Brandt-Rauf, P. W., and Fine, R. L. (2002) *Biochem. Biophys. Res. Commun.* **298,** 439–449
33. Nakano, H., Nakajima, A., Sakon-Komazawa, S., Piao, J. H., Xue, X., and Okumura, K. (2006) *Cell Death Differ.* **13,** 730–737
34. Johnson, T. M., Yu, Z. X., Ferrans, V. J., Lowenstein, R. A., and Finkel, T. (1996) *Proc. Natl. Acad Sci. U. S. A.* **93,** 11848–11852
35. Maianski, N. A., Roos, D., and Kuijpers, T. W. (2003) *Blood* **101,** 1987–1995
36. Shih, C. M., Ko, W. C., Wu, J. S., Wei, Y. H., Wang, L. F., Chang, E. E., Lo, T. Y., Cheng, H. H., and Chen, C. T. (2004) *J. Cell. Biochem.* **91,** 384–397
37. Mates, J. M., and Sanchez-Jimenez, F. M. (2000) *Int. J. Biochem. Cell Biol.* **32,** 157–170
38. Raha, S., and Robinson, B. H. (2001) *Am. J. Med. Genet.* **106,** 62–70

Activation of Targeted Necrosis by a p53 Peptide: A NOVEL DEATH PATHWAY THAT CIRCUMVENTS APOPTOTIC RESISTANCE

Richard D. Dinnen, Lisa Drew, Daniel P. Petrylak, Yuehua Mao, Nicholas Cassai, Joseph Szmulewicz, Paul Brandt-Rauf and Robert L. Fine

J. Biol. Chem. 2007, 282:26675-26686.
doi: 10.1074/jbc.M701864200 originally published online July 18, 2007
